JOURNAL OF SPACECRAFT AND ROCKETS
Vol. 32, No. 2, March–April 1995

Evaluation of a Multigrid-Based Navier–Stokes Solver for Aerothermodynamic Computations

Veer N. Vatsa*
NASA Langley Research Center, Hampton, Virginia 23681-0001

A multigrid acceleration technique developed for solving the three-dimensional Navier–Stokes equations is used for computing high-Mach-number flows over configurations of practical interest. An explicit multistage Runge–Kutta time-stepping scheme is used as the basic algorithm. Solutions are presented for a spherically blunted cone at Mach 10 and a modified Shuttle orbiter at Mach 6. The computed surface heat-transfer distributions are shown to compare well with the experimental data. Effect of grid refinement on computed heat-transfer distributions is also examined to assess the numerical accuracy of the computed solutions. The rapid convergence rate associated with multigrid schemes in previous applications at transonic speeds is observed at the higher-Mach-number flows investigated here.

Nomenclature

C_L	= lift coefficient
D	= sum of dissipative and viscous fluxes
d	= artificial dissipation term
E	= energy per unit volume
F, G, H	= components of convective flux vector in stream, normal, and span directions
G_v	= viscous flux component in normal direction
i, j, k	= coordinate indices in ξ, η, and ζ directions
J	= Jacobian of transformation
l, L	= length of body, meters
M	= Mach number
p	= static pressure
Q	= sum of convective fluxes
q	= heat-transfer coefficient, W/cm^2
s	= circumferential arc length, m
$s_{\max}$	= maximum arc length in circumferential direction, m
T_1, T_2	= parameters for shock detection switch
t	= time
U	= dependent-variable vector
u, v, w	= Cartesian velocity components, m/s
W	= a typical conserved variable
x_s	= streamwise distance measured from apex of equivalent sharp cone, m
α	= angle of attack, deg
$\epsilon^{(2)}$	= multiplicative coefficient for second-order dissipation
$\epsilon^{(4)}$	= multiplicative coefficient for fourth-order dissipation
$\kappa^{(2)}$	= scaling constant for second-order dissipation
$\kappa^{(4)}$	= scaling constant for fourth-order dissipation
λ	= eigenvalue used in dissipation scaling
ν	= pressure-gradient parameter defined in Eq. (6)
ξ, η, ζ	= curvilinear coordinates along stream, normal, and span directions
ω	= weight factor used in construction of shock detection switch

Subscripts

∞	= freestream value
0	= stagnation value
max	= maximum value
w	= wall value

Introduction

DURING the last decade, progress made in the field of computational fluid dynamics (CFD) has significantly influenced the design and analysis of aerodynamic configurations. Solutions of the Euler (inviscid) equations for essentially complete aircraft configurations[1–4] and the solutions of the Navier–Stokes equations for high-Reynolds-number, viscous, transonic flows over aircraft components are now available in the open literature.[5–9] Most of the efficient numerical schemes for solving aerodynamic flows rely on multigrid acceleration techniques[2,8,9] to enhance the convergence rate. The multigrid-based schemes have the desirable property that the number of iterations required to achieve a steady-state solution is nearly independent of the mesh size for a given class of problems. Thus one can achieve grid-converged, steady-state solutions, even for the numerically demanding problem of high Reynolds-number, transonic, viscous flow over aircraft components, with a reasonable amount of computer resources.[9]

Despite the progress achieved in solving transonic flows, the development of efficient CFD methods for supersonic and hypersonic flows seems to be lagging at the present time. Most numerical schemes currently in use for high-speed flows require a prohibitive amount of computer time to obtain converged solutions.[10,11] A notable exception is the progress reported in the development of multigrid-based schemes[12–15] for two- and three-dimensional high-speed flows within the last few years. In this paper, we will discuss the application of a computationally efficient, multigrid-based central-difference algorithm known as TLNS3D[9,15] to aerothermodynamic problems. Sample results for problems of practical interest will be presented along with comparisons with experimental data to evaluate the accuracy of the numerical solutions.

Governing Equations and Numerical Method

The basic equations under consideration are the unsteady Navier–Stokes equations. These are specialized to a body-fitted coordinate system (ξ, η, ζ), where ξ, η, and ζ represent the streamwise, normal, and spanwise coordinates, respectively. The η coordinate lines are nearly orthogonal to the wing surface. Since the dominant viscous effects for high-Reynolds-number flows arise from viscous diffusion normal to the body surface, a thin-layer assumption is employed here by retaining only the viscous diffusion terms in the

Presented as Paper 92-4563 at the AIAA Atmospheric Flight Mechanics Conference, Hilton Head, SC, Aug. 10–12, 1992; received July 1, 1993; revision received June 29, 1994; accepted for publication June 30, 1994. Copyright © 1995 by the American Institute of Aeronautics and Astronautics, Inc. No copyright is asserted in the United States under Title 17, U.S. Code. The U.S. Government has a royalty-free license to exercise all rights under the copyright claimed herein for Governmental purposes. All other rights are reserved by the copyright owner.

*Senior Research Scientist, AAMB, FMAD, Mail Stop 128. Member AIAA.

η direction. These equations can be written in the conservation-law form as

$$\frac{\partial}{\partial t}(J^{-1}U) + \frac{\partial F}{\partial \xi} + \frac{\partial G}{\partial \eta} + \frac{\partial H}{\partial \zeta} = \frac{\partial G_v}{\partial \eta} \tag{1}$$

where the dependent variable vector U is given by the relation

$$U = \begin{Bmatrix} \rho \\ \rho u \\ \rho v \\ \rho w \\ \rho E \end{Bmatrix} \tag{2}$$

In Eq. (1), F, G, G_v, and H are the flux vectors, and J is the Jacobian of the transformation. The effects of turbulence are incorporated in the governing equations through the eddy-viscosity and eddy-conductivity concepts modeled via the Baldwin–Lomax turbulence model. The complete forms of these quantities are readily available.[9]

A pseudo-time-stepping procedure based on a Runge–Kutta scheme[16,17] is used for integrating the time-dependent equations to steady state and also as a smoother in the multigrid scheme. For convenience, the discretized form of the governing equations is written in the following operator notation:

$$\frac{\mathrm{d}}{\mathrm{d}t}(J^{-1}U) + Q(U) - D(U) = 0 \tag{3}$$

where Q contains all the convective and viscous fluxes and D represents the artificial dissipative fluxes.

Since our primary interest here is to obtain solutions for viscous flows via the Navier–Stokes equations, both the diffusion and the convective terms are important, in contrast with the Euler equations, where convective terms are dominant. Therefore, it is preferable to employ a scheme that has good stability properties along both the real and imaginary axes for accommodating the complete range of convection- and diffusion-dominated problems. Based on the Fourier stability analysis of a one-dimensional model problem,[18] the five-stage Runge–Kutta scheme, with three evaluations of the dissipative operator at the first, third, and fifth stages, appears very attractive and is employed in the present work. The convergence to steady state is enhanced via the use of local time-stepping and implicit residual smoothing techniques,[16,17] with variable coefficients for the residual smoothing.[9] All the computations in this paper were performed with a CFL number of 4.5.

Boundary Conditions

At the far-field boundaries, a test is performed on the velocity component normal to the boundary. For an inflow boundary, all the flow variables are set to their freestream values. For an outflow boundary, all the variables are extrapolated from the interior. On the solid surface, a no-slip boundary condition is imposed by setting all the velocity components to zero. A zero pressure gradient and specified value of wall temperature are also imposed on the solid surface.

Artificial Dissipation Model

The artificial dissipation model used in this study is closely related to the dissipation model developed for transonic flows.[9,16,17] The modifications required for supersonic and hypersonic viscous flows were described in an earlier paper[15] and are discussed here briefly for completeness. The first and third differences constituting the artificial dissipation in the i direction can be written as follows:

$$\frac{d_{i+\frac{1}{2},j,k}}{\lambda_{i+\frac{1}{2},j,k}} = \epsilon^{(2)}_{i+\frac{1}{2},j,k}(W_{i+1,j,k} - W_{i,j,k})$$

$$- \epsilon^{(4)}_{i+\frac{1}{2},j,k}(W_{i+2,j,k} - 3W_{i+1,j,k} + 3W_{i,j,k} - W_{i-1,j,k}) \tag{4}$$

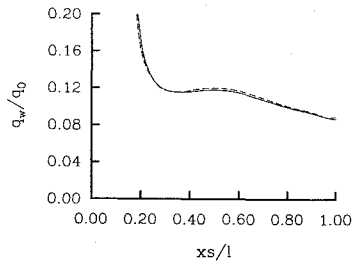

a) Windward side

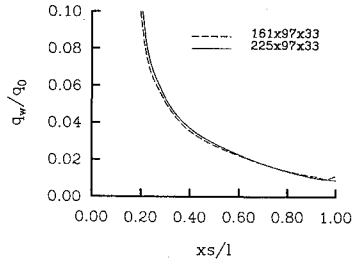

b) Leeward side

Fig. 1 Effect of streamwise grid variation on heat-transfer distribution for a blunt cone.

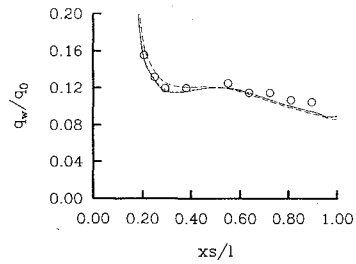

a) Windward side

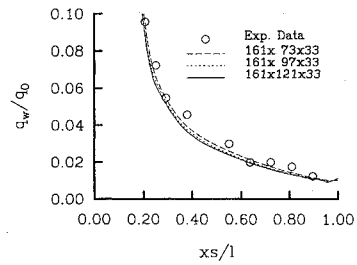

b) Leeward side

Fig. 2 Heat-transfer comparisons for a blunt cone.

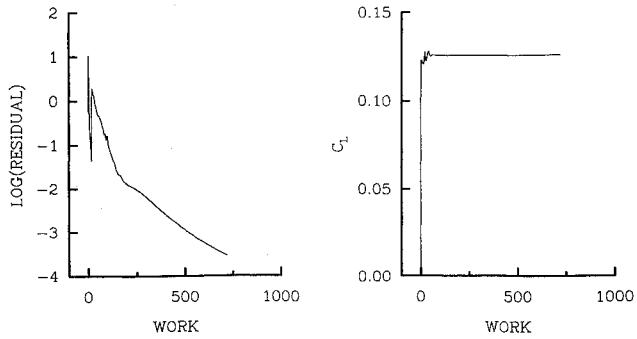

Fig. 3 Convergence history for a blunt cone and a 161 × 121 × 33 grid.

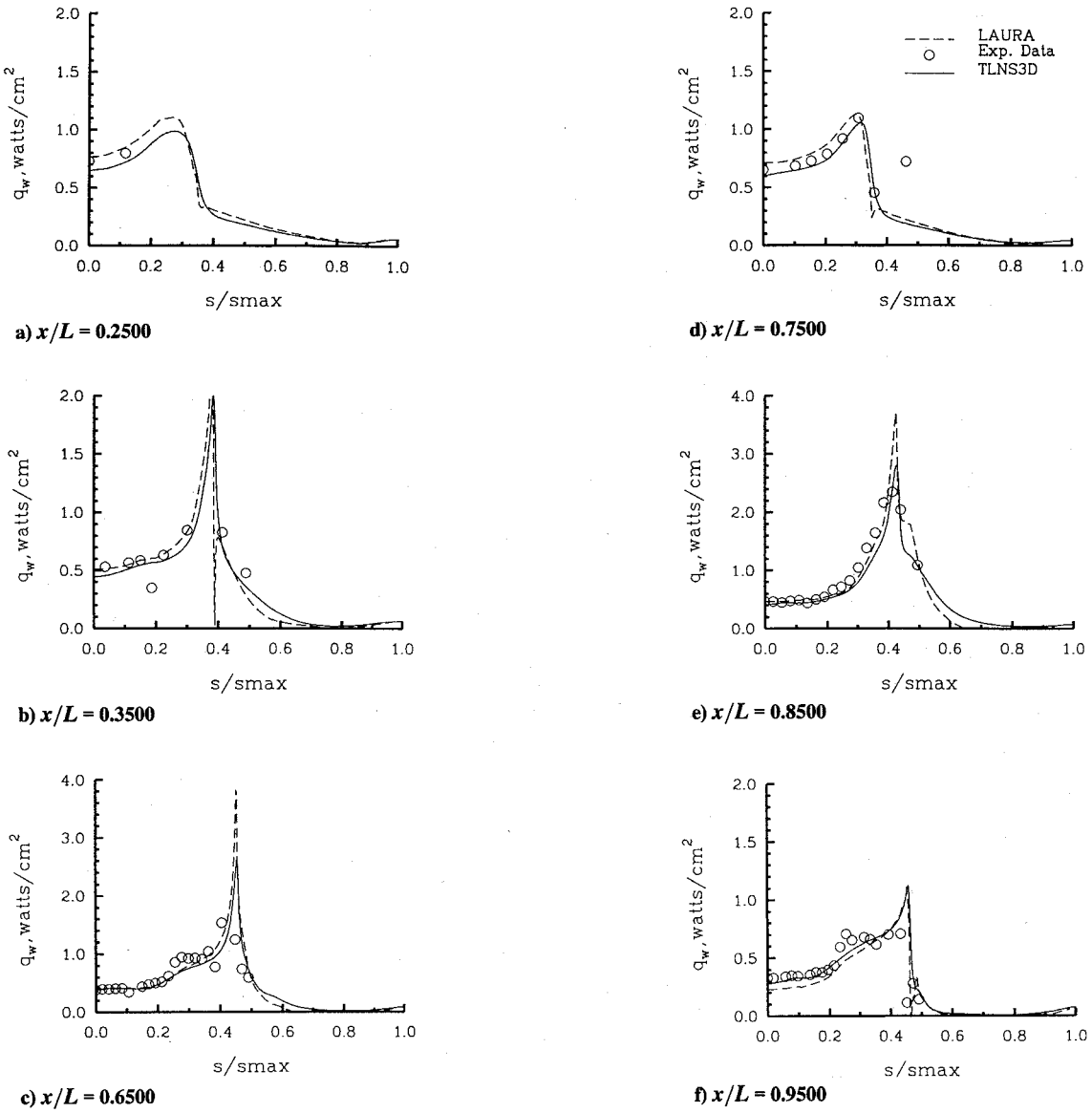

Fig. 4 Comparison of heat-transfer coefficients for the modified Shuttle orbiter (M_∞ = 5.83, Re_l = 4.5 × 10^5, α = 30 deg).

In Eq. (4), $\lambda_{i+1/2,j,k}$ is a modified eigenvalue scaling factor,[9] and the coefficients $\epsilon^{(2)}_{i+1/2,j,k}$ and $\epsilon^{(4)}_{i+1/2,j,k}$ are related to the pressure gradient as follows:

$$\epsilon^{(2)}_{i+\frac{1}{2},j,k} = \kappa^{(2)} \max(\nu_{i+1}, \nu_i)$$

$$\epsilon^{(4)}_{i+\frac{1}{2},j,k} = \max\left\{0, \left(\kappa^{(4)} - \epsilon^{(2)}_{i+\frac{1}{2},j,k}\right)\right\} \tag{5}$$

where the coefficients $\kappa^{(2)}$ and $\kappa^{(4)}$ are set equal to $\frac{1}{2}$ and $\frac{1}{64}$, respectively. The quantities ν_i depend on the pressure-gradient parameter and are modified to produce a TVD variation of the shock-detection switch[19] in the following manner:

$$\nu_i = \frac{|p_{i+1,j,k} - 2p_{i,j,k} + p_{i-1,j,k}|}{(1-\omega)T_1 + \omega T_2}$$
$$T_1 = |p_{i+1,j,k} - p_{i,j,k}| + |p_{i,j,k} - p_{i-1,j,k}| \tag{6}$$
$$T_2 = p_{i+1,j,k} + 2p_{i,j,k} + p_{i-1,j,k}$$

Note that by setting $\omega = 1$, we can recover the shock switch developed for transonic flow computations.[9,16,17] For supersonic and hypersonic flows, $\omega = \frac{1}{2}$ is found to give satisfactory results.

Multigrid Acceleration Technique

In the current application, the full-approximation storage (FAS) scheme of Brandt[20] is used in conjunction with the multigrid strategy devised by Jameson[18] for the solution of the Euler equations. The extensions for three-dimensional supersonic and hypersonic viscous flows[15] are used in this investigation. A five-stage Runge–Kutta scheme with coefficients selected to provide good damping of the high-frequency errors is employed. The restriction operator used to transfer the solution to a coarser grid is a volume-weighted average of the eight surrounding cell-centered values. The forcing function for a cell on the coarse grid is obtained by simply summing the residuals of its constituent fine-grid cells. The corrections are transferred from the coarse grid back to the fine grid (or prolonged) by simple trilinear interpolation in the computational space. On highly stretched or nonuniform grids, this prolongation operator can introduce high-frequency errors back into the fine grid, causing degradation of the convergence rate. To prevent this degradation, the coarse-grid corrections are processed through an implicit residual smoothing operator before being added to the fine-grid corrections. Whereas the smoothing of the coarse-grid corrections is certainly helpful for transonic flow calculations, it is essential for obtaining converged solutions for higher-speed flows.

The solutions presented in this paper were obtained using a W cycle, in which the governing equations are solved only in the

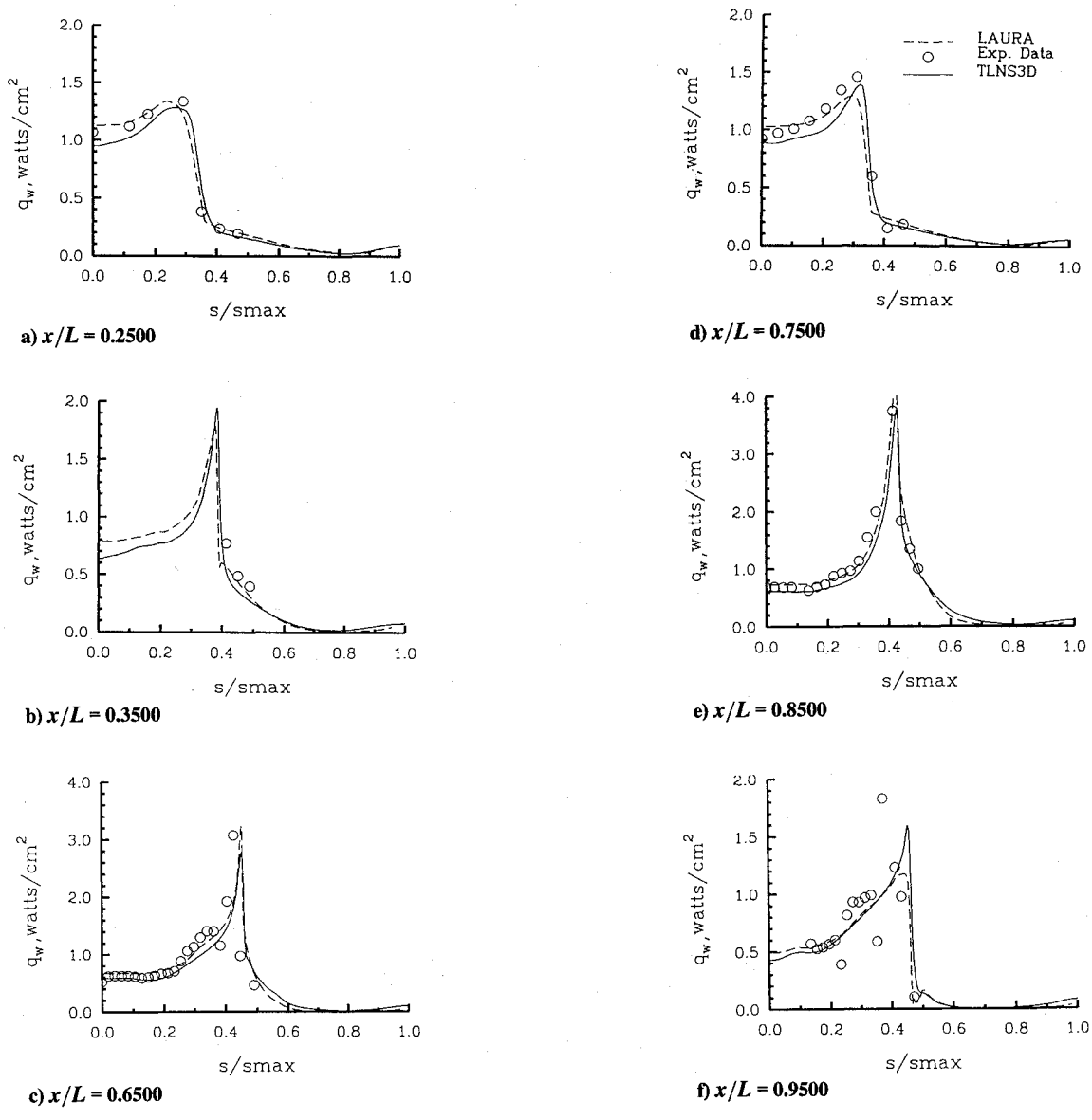

Fig. 5 Comparison of heat-transfer coefficients for the modified Shuttle orbiter (M_∞ = 5.83, $Re_l = 4.5 \times 10^5$, α = 40 deg).

restriction step. The W cycle resulted in approximately a 25% reduction in computational time from a standard V cycle for achieving comparable convergence levels of the residuals. In addition, global properties, such as lift and drag, develop more rapidly with the W cycle, since more time is spent on the coarser grids. It is also helpful to run more cycles on coarser grid levels for supersonic and hypersonic flows to better establish and precondition the flowfield before starting computations on the finest mesh in the full multigrid (FMG) cycle.

The variable-coefficient residual smoothings are applied on all grid levels of the multigrid cycle. On the finest grid, the blend of second- and fourth-difference artificial dissipation discussed previously is employed. For the coarser grids, a fixed-coefficient second-difference dissipation model has been replaced by a pressure-gradient-based dissipation model employing a TVD switch [Eqs. (5 and 6)] to improve the convergence rate of the present scheme in supersonic and hypersonic flow regimes.

Results and Discussion

Two test cases encompassing supersonic to low hypersonic speed regimes were selected to evaluate the applicability of the multigrid-based Navier–Stokes code TLNS3D to aerothermodynamic problems of practical interest. Since the configurations under consideration have blunt noses, C-O grids are used to provide good resolution in the leading-edge regions. The accuracy of the computed solutions is assessed via comparisons with available experimental data and other numerical solutions.

Spherically Blunted Cone

The first test case chosen for this study is a simple aerodynamic shape obtained by adding a spherical cap to a 15-deg cone. Cleary[21] has conducted an extensive experimental study to determine the effects of angle of attack and bluntness on the heating rate of blunted cones at $M_\infty = 10.6$. In this paper, the configuration with a bluntness ratio (nose radius/base radius) of 0.183 is examined. Computations are performed for an angle of attack α of 5 deg and a Reynolds number Re_n of 136,400 (based on the nose radius), corresponding to one of the test conditions investigated.[21] Since a classical grid-refinement study with grid doubling in all three coordinate directions is impractical on account of memory limitations even on the current supercomputers, a limited grid-refinement study has been conducted to assess the adequacy of the grids employed herein, starting with a 161 × 97 × 33 mesh as the baseline grid. As a first step, the effect of grid refinement in the streamwise direction is investigated. For this exercise, two different grids are used, consisting of 161 and 225 nodes in the streamwise direction with 97 × 33 nodes in the normal and circumferential directions. The computed heat-transfer rates for this case are normalized[21] by the stagnation heating rate q_0. The variation in the streamwise mesh has only a small effect on the computed heat-transfer distributions,

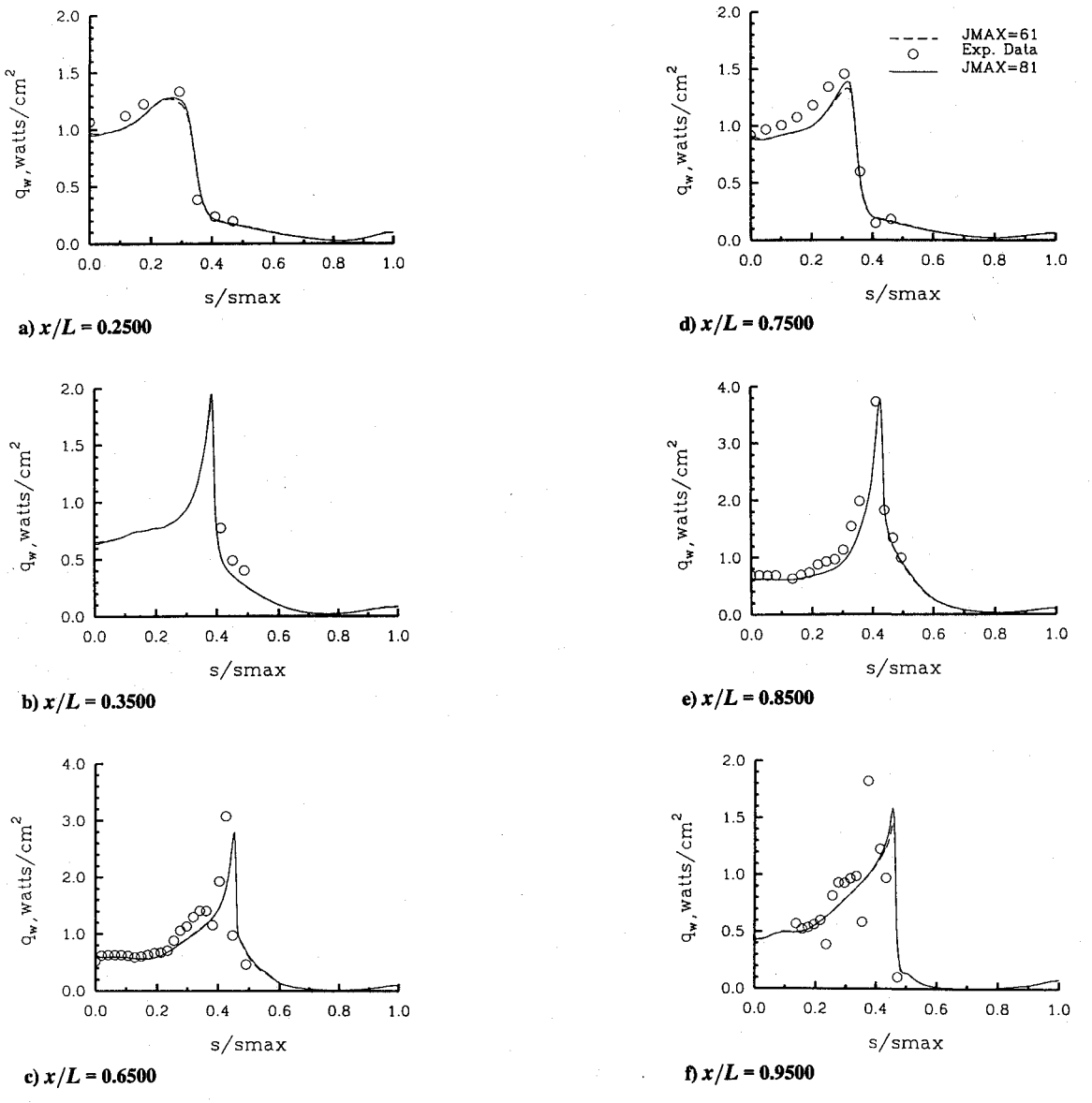

Fig. 6 Effect of normal mesh-density variation on heat-transfer coefficients for the modified Shuttle orbiter (M_∞ = 5.83, $Re_l = 4.5 \times 10^5$, α = 40 deg).

as shown in Fig. 1. The effect of varying the circumferential mesh from 25 to 37 nodes (50% variation) was also found to be insignificant (results not shown) for the predicted heat-transfer distributions. Based on this exercise, it appears that the tangential mesh consisting of 161 × 33 points used here is adequate for accurate predictions of heat transfer for this case.

Since the heat-transfer coefficient is usually most sensitive to the normal mesh density, a more detailed study is conducted to assess the effect of varying the mesh in the normal (boundary layer) direction. Solutions were obtained with 73, 97, and 121 nodes in the normal direction in conjunction with a tangential mesh consisting of 161 × 33 nodes in the streamwise and circumferential directions. In Fig. 2, the computed surface heat-transfer coefficients on the windward and leeward sides are compared with the experimental data of Ref. 21. The effect of refining the normal mesh density beyond 97 points is minimal, and the computed solutions on the two finest meshes used here are essentially identical. The agreement between the computed results (for 97 or more points in the normal direction) and the experimental data is considered quite good, thereby demonstrating the feasibility of the present central-difference scheme for accurate prediction of heat-transfer distributions for high-Mach-number flows.

The efficiency of the present scheme is demonstrated by examining the convergence history of the numerical solutions. Figure 3 shows the time evolution of the residual of continuity equation and the lift coefficient from computations on the 161 × 121 × 33 mesh, using a W-cycle of the multigrid. The convergence rates from the coarser mesh computations (not shown) are slightly better than the results shown in Fig. 3. Although the convergence rate observed in Fig. 3 appears to be somewhat slower than in the computations of turbulent, transonic flow,[9] it is believed to be significantly better than the convergence rate associated with nonmultigrid schemes.

Modified Shuttle Orbiter

A modified Shuttle orbiter, popularly known as "Halis," is the second test case chosen for evaluating the TLNS3D code for aerothermodynamic problems. In the present investigation, C-O grids created for this problem in an earlier study[10] are employed. Significant grid clustering is used in the thin region adjacent to the solid surface in order to resolve the thin shear layers present in high-Reynolds-number flows. In addition, the outer boundaries are placed outside the bow shock generated by the blunt nose.

The test conditions chosen for this study are a Mach number M_∞ of 5.83, and a Reynolds number Re_l of 4.5×10^5 based on the model length. The computations are performed at 30- and 40-deg angles of attack α, corresponding to two of the test conditions used in the experimental study.[22] The grids used for these computations are identical to the ones used by Hamilton et al.,[10] except in the 30-deg case, where one layer of cells in the normal direction had to be

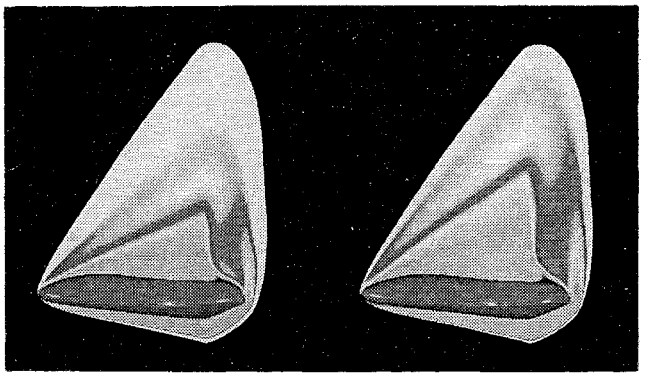

a) $\alpha = 30°$ b) $\alpha = 40°$

Fig. 7 Effect of angle of attack on the flowfield for the modified Shuttle orbiter.

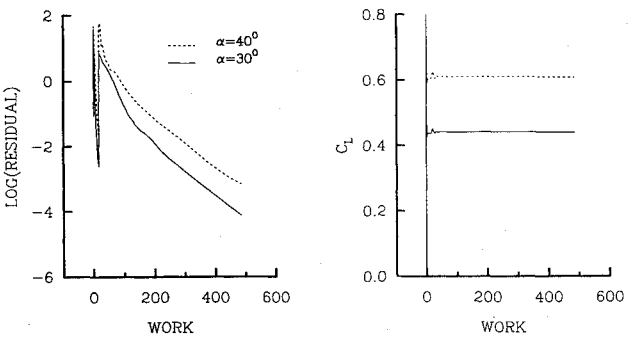

Fig. 8 Convergence history for the modified Shuttle orbiter.

eliminated to produce a multigriddable mesh. Thus, grids consisting of 289 × 69 × 41 and 289 × 81 × 41 mesh points were employed in these computations for the 30- and 40-deg cases, respectively.

The computed surface heat-transfer coefficient distributions are shown in Figs. 4 and 5 at six streamwise stations for these cases. The experimental data and computational results from an earlier study based on a flux-difference-splitting code LAURA[10] are also shown in this figure. A comparison of the two prediction methods shows good correlation except near the wing-tip region, where the solutions of Ref. 10 display sharp discontinuity in heat-transfer distributions. Such nonphysical behavior may be caused by the flux limiters used in the scheme.[10] The present solutions compare well with the experimental data all the way from the windward to the leeward side of this configuration, with the agreement improving slightly at the downstream stations. Given the scatter in the experimental data, present results compare favorably with the experimental data of Ref. 22, and with the results from the flux-difference scheme of Ref. 10.

A limited grid-refinement study was conducted for the 40-deg case to study the effect of normal mesh density. A coarser mesh with 61 points in the normal direction was generated by a redistribution of the points from the baseline mesh, which contained 81 points in that direction. The results from this study are shown in Fig. 6. These comparisons indicate that the overall effect of refining the normal mesh is a slight increase in the predicted heat-transfer coefficients due to better resolution of the boundary layer. This is more evident in the wing-tip region, where the boundary layer becomes very thin because of strong acceleration of the flow from the lower to the upper surface and the computations display the largest effect of grid refinement. Thus it appears that the correlation with the experimental data will improve slightly on a finer normal mesh; however, the normal mesh density of the baseline mesh is considered adequate over most of this configuration.

The Mach contours in the symmetry and downstream planes are presented in Fig. 7 to show the effect of increase in angle of attack on the overall flowfield and shock positions. It is observed from this figure that the bow shock developing at the blunt nose almost hugs the lower surface (windward plane), whereas on the upper surface (leeward side), it extends very far from the body at the angles of attack considered here. Such conflicting requirements are very demanding on the mesh generation and the numerical code, since we need not only to resolve the large gradients present in the thin shock layer on the lower surface, but also to capture the bow shock, which is almost a body length away from the upper surface. Nonetheless, the solutions shown here clearly display a well-resolved shock structure in the symmetry and crossflow planes. As expected, the bow shock and the crossflow shocks on the upper surface move further away from the solid surface with an increase in angle of attack. On the lower surface, the bow shock is much closer to the surface; however, the mesh extends far enough on both the windward and leeward sides to capture the bow shocks.

To demonstrate the most significant advantage of the present scheme, the convergence history in terms of residual error of the continuity equation and the lift coefficient for these cases is shown in Fig. 8 as a function of work units. A work unit represents the computational effort required for one fine-mesh iteration. A total of 300 iterations (485 work units) were performed on the fine grid, which resulted in approximately 5 orders of magnitude reduction in the residual. The lift and drag for this case converged to within 0.1% of their final value in less than 100 fine-grid iterations. These computations required 2.85 h of CPU time for the 30-deg case (289×69×41 grid), and 3.2 h for the 40-deg case (289×81×41 grid), on a Cray Y-MP supercomputer. These computational requirements are approximately an order of magnitude smaller than with nonmultigrid codes (see, e.g., Ref. 10) currently being used for such problems.

Concluding Remarks

A multigrid-based Navier–Stokes solver has been applied to solve high-angle-of-attack supersonic and hypersonic flows over a blunt cone and a modified Shuttle orbiter. The computed heat-transfer distributions compare well with the experimental data for both test cases and also with previous calculations for the Shuttle orbiter. The present code offers an order-of-magnitude reduction in computer time for obtaining steady-state solutions for such problems below that required by nonmultigrid codes. Based on these solutions, it is concluded that the resulting code is capable of accurately predicting high-speed viscous aerothermodynamic problems in an efficient manner.

Acknowledgment

The author would like to express his appreciation to Frank Greene of NASA Langley Research Center for providing the computational grids, and the flux-difference scheme solutions for the modified Shuttle orbiter, used in this paper.

References

[1]Sawada, K., and Takanashi, S., "A Numerical Investigation on Wing/Nacelle Interferences of USB Configurations," AIAA Paper 87-0455, Jan. 1987.

[2]Jameson, A., and Baker, T. J., "Multigrid Solution of the Euler Equations for Aircraft Configurations," AIAA Paper 84-0093, Jan. 1984.

[3]Jameson, A., and Baker, T. J., "Improvements to the Aircraft Euler Method," AIAA Paper 87-0452, Jan. 1987.

[4]Yu, N. J., Kusunose, K., Chen, H. C., and Summerfield, D. M., "Flow Simulations for a Complex Airplane Configuration Using Euler Equations," AIAA Paper 87-0454, Jan. 1987.

[5]Agarwal, R. K., and Deese, J. E., "Computation of Transonic Viscous Airfoil, Inlet, and Wing Flowfields," AIAA Paper 84-1551, June 1984.

[6]Kaynak, U., and Flores, J., "Advances in the Computation of Transonic Separated Flows over Finite Wings," AIAA Paper 87-1195, June 1987.

[7]Vatsa, V. N., Wedan, B. W., and Turkel, E., "3-D Euler and Navier–Stokes Calculations for Aircraft Components," NASA CP-3020, 1989.

[8]Thomas, J. L., Krist, S. T., and Anderson, W. K., "Navier–Stokes Computations of Vortical Flows over Low-Aspect-Ratio Wings," *AIAA Journal*, Vol. 28, No. 2, 1990, pp. 205–212.

[9]Vatsa, V. N., and Wedan, B. W., "Development of a Multigrid Code for 3-D Navier–Stokes Equations and Its Application to a Grid-Refinement Study," *Computers and Fluids*, Vol. 18, No. 2, 1990, pp. 391–403.

[10]Hamilton, H. H., II, Greene, F. A., and Weilmuenster, K. J., "Comparison of Heating Rate Calculations with Experimental Data on a Modified Shuttle Orbiter at Mach 6," AIAA Paper 91-1347, June 1991.

[11]Desideri, J. A., and Periaux, J. (eds.), *Proceedings of the Workshop on Hypersonic Flows for Reentry Problems*, Vol. 2, Springer-Verlag, Antibes, 1990, pp. 472–493.

[12]Radespiel, R., and Kroll, N., "Multigrid Schemes with Semicoarsening for Accurate Computations of Hypersonic Viscous Flows," IB 129-90/19, Institut für Entwurfsaerodynamik, Braunschweig, Germany, April 1991.

[13]Thomas, J. L., "An Implicit Multigrid Scheme for Hypersonic Strong-Interaction Flowfields," *Communications in Applied Numerical Methods*, Vol. 8, No. 9, Sept. 1992.

[14]Turkel, E., Swanson, R. C., Vatsa, V. N., and White, J. W., "Multigrid for Hypersonic Viscous Two- and Three-Dimensional Flows," AIAA Paper 91-1572, June 1991.

[15]Vatsa, V. N., Turkel, E., and Abolhassani, J. S., "Extension of Multigrid Methodology to Supersonic/Hypersonic 3-D Viscous Flows," *International Journal of Numerical Methods in Fluids*, Vol. 17, No. 10, 1993, pp. 825–837.

[16]Jameson, A., Schmidt, W., and Turkel, E., "Numerical Solutions of the Euler Equations by Finite Volume Methods Using Runge–Kutta Time-Stepping Schemes," AIAA Paper 81-1259, June 1981.

[17]Jameson, A., and Baker, T. J., "Solution of the Euler Equations for Complex Configurations," AIAA Paper 83-1929, July 1983.

[18]Jameson, A., "Solution of the Euler Equations by a Multigrid Method," *Applied Mathematics and Computation*, Vol. 13, No. 3–4, 1983, pp. 327–356.

[19]Swanson, R. C., and Turkel, E., "On Central-Difference and Upwind Schemes," Report 90-44, Institute of Computer Applications in Science and Engineering, Hampton, VA, June 1990.

[20]Brandt, A., "Multi-level Adaptive Solutions to Boundary-Value Problems," *Mathematics of Computation*, Vol. 31, April 1977, pp. 333–390.

[21]Cleary, J. W., "Effects of Angle of Attack and Bluntness on Laminar Heating-Rate Distributions of a 150 Cone at a Mach Number 10.6," NASA TN D-5450, Oct. 1969.

[22]Micol, J., "Aerothermodynamic Measurement and Prediction for Modified Orbiter at Mach 6 and 10," AIAA Paper 91-1436, June 1991.

K. J. Weilmuenster
Associate Editor

Notice to Authors and Subscribers:

Beginning early in 1995, AIAA will produce on a quarterly basis a CD–ROM of all *AIAA Journal* papers accepted for publication. These papers will not be subject to the same paper- and issue-length restrictions as the print versions, and they will be prepared for electronic circulation as soon as they are accepted by the Associate Editor.

AIAA Journal on Disc

This new product is not simply an alternative medium to distribute the *AIAA Journal*.

- Research results will be disseminated throughout the engineering and scientific communities much more quickly than in the past.
- The CD–ROM version will contain fully searchable text, as well as an index to all AIAA journals.
- Authors may describe their methods and results more extensively in an addendum because there are no space limitations.

The printed journal will continue to satisfy authors who want to see their papers "published" in a traditional sense. Papers still will be subject to length limitations in the printed version, but they will be enhanced by the inclusion of references to any additional material that is available on the CD–ROM.

Authors who submit papers to the *AIAA Journal* will be provided additional CD–ROM instructions by the Associate Editor.

If you would like more information about how to order this exciting new product, send your name and address to:

AIAA
American Institute of Aeronautics and Astronautics

AIAA Customer Service
370 L'Enfant Promenade, SW
Washington, DC 20024-2518
Phone 202/646-7400
FAX 202/646-7508